European Journal of Mechanics A/Solids 59 (2016) 58–66

Contents lists available at ScienceDirect

European Journal of Mechanics A/Solids

journal homepage: www.elsevier.com/locate/ejmsol

Application of the Coupled Eulerian-Lagrangian (CEL) method to the modeling of orthogonal cutting

F. Ducobu*, E. Rivière-Lorphèvre, E. Filippi

University of Mons (UMONS), Faculty of Engineering (FPMs), Machine Design and Production Engineering Lab, 20 Place du Parc, B-7000, Mons, Belgium

ARTICLE INFO

Article history:
Received 25 March 2015
Received in revised form
28 January 2016
Accepted 15 March 2016
Available online 18 March 2016

Keywords:
Chip formation
Coupled Eulerian-Lagrangian (CEL)
Orthogonal cutting

ABSTRACT

Numerical modeling of metal cutting is a complex problem involving many nonlinear and coupled phenomena (high speed, large strains, large strain-rates, heat generation, etc.). Due to the large deformations, the mesh of the workpiece is often highly distorted. When it does not ends prematurely the computing, it slows it down and decreases the confidence in the results. Many formalisms are encountered in the literature to model the orthogonal cutting process, each with their pros and cons, more or less significant. This paper introduces the Coupled Eulerian-Lagrangian (CEL) formulation, in which the workpiece is described by the Eulerian formulation and the tool by the Lagrangian one. The comparison with experimental results and an Arbitrary Lagrangian-Eulerian (ALE) model with pure Lagrangian boundaries shows that the chip morphology and the cutting forces are well predicted by that new model. The absence of mesh deformation in the part does not decrease the stable time increment and therefore does not slow down the computing, which is competitive compared to the reference ALE model. This also increases confidence in the results given by the CEL model and opens new possibilities in the modeling of metal cutting.

1. Introduction

Numerical modeling of metal cutting is used since the beginning of the seventies in the simplified configuration of (2D) orthogonal cutting (Pantalé et al., 2004). However, developing an accurate and computing efficient model is not easy and many ways of modeling have been tested in the literature. Most of the finite element models are providing information such as temperatures at the tool–chip interface (Maranhão and Davim, 2010; Jackson et al., 2010), shear stresses (Maranhão and Davim, 2010), plastic strain and plastic strain rate (Maranhão and Davim, 2010; Davim and Maranhão, 2009) or residual stresses in the machined workpiece (Maranhão and Davim, 2010; Arrazola et al., 2014), some of them being experimentally measured with difficulty.

Initially, two types of models, Eulerian and Lagrangian ones, were encountered due to the two primary mathematical formulations in the finite element method (Pantalé et al., 2004). In the Eulerian formulation, the mesh is fixed in space and the material moves through it, while the mesh deforms with the material in the Lagrangian formulation. The Eulerian formulation is the classical approach in fluid dynamics. A pure Eulerian model can only be used if the machining process is in a steady-state and requires to know the final chip geometry as an assumption, which are major disadvantages (Arrazola et al., 2013). Despite the severe elements deformation, the Lagrangian formulation (i.e. the classical approach in solid mechanic) has been extensively used to model the unsteady-state orthogonal metal cutting (Arrazola et al., 2013). This type of models requires a criterion, the “chip separation criterion”, to enable for the chip to come off the workpiece (Pantalé, 2005; Heinstein and Segalman, 1997; Yvonnet, 2004). It influences the chip formation notably and it should be carefully chosen (Pantalé et al., 2004). This criterion can be based on a geometrical method (Li et al., 2002; Ohbuchi and Obikawa, 2003) with a separation line composed of superimposed nodes defined before computing the model or on a physical (or “erosion”) method (Subbiah and Melkote, 2008) in which the elements satisfying a criteria (maximal plastic strain (Obikawa et al., 1997), damage (Owen and Vaz Jr., 1999), etc.) are deleted. Again, two alternatives are observed: either the elements to be deleted are defined initially and constitute a “sacrificial layer” (Subbiah and Melkote, 2008; Mabrouki and Rigal, 2006; Zhang et al., 2011a), either any element of the mesh is given the property to be deleted (Pantalé

* Corresponding author.
E-mail address: Francois.Ducobu@umons.ac.be (F. Ducobu).

http://dx.doi.org/10.1016/j.euromechsol.2016.03.008
0997-7538/

et al., 2004; Simoneau et al., 2006, 2007; Ghadbeigi et al., 2009). Remeshing can be adopted to reduce mesh distortion (Umbrello, 2008; Schulze and Zanger, 2011; Bäker et al., 2002). A chip criterion is then not required anymore for the chip to be formed. It however leads to a significant increase in the CPU computing time and decreases the results accuracy because of the approximations needed to transfer the values from the old mesh to the new one (Heinstein and Segalman, 1997; Skrzat, 2012).

The Arbitrary Lagrangian-Eulerian (ALE) formulation combines the advantages of the Eulerian and Lagrangian formulations to limit the mesh distortions thanks to the relative movement of the mesh while containing the CPU computing time (Pantalé et al., 2004; Arrazola and Özel, 2010). It is usually considered that the chip formation occurs because of the material plastic flow around the tool (Woon et al., 2007) and no chip criterion has to be introduced in that type of models (Özel and Zeren, 2007a). An ALE model with Eulerian and Lagrangian boundaries will be used to solve steady-state problems (Özel and Zeren, 2007b), while an ALE model with pure Lagrangian boundaries will focus on the transient chip formation (Özel and Zeren, 2005, 2007a), like a Lagrangian model. In an ALE model with Eulerian and Lagrangian boundaries, the chip has to be preformed (like in a pure Eulerian model). The first estimation of the chip morphology is usually carried out by trials and errors. Noticeable advantages of an ALE model with Eulerian and Lagrangian boundaries are that it allows to model long duration cutting and a refined mesh is easily used in the primary and secondary shear zones (Courbon et al., 2013; Arrazola et al., 2008). The ALE technique is usually faster than remeshing but highly deformed elements can still be formed when the mesh is not able to adapt itself sufficiently (Arrazola et al., 2007). Because of the relative displacement between the mesh and the material, an ALE model with pure Lagrangian boundaries does not lead to a chip with a geometry close to the experimental one when segmented (or saw-toothed) chip is observed, contrary to a Lagrangian model (Ducobu et al., 2014).

In order to overcome these disadvantages, this paper presents the application of the Coupled Eulerian-Lagrangian (CEL) technique to orthogonal metal cutting. It involves both Eulerian and Lagrangian formulations (Skrzat, 2012). It is typically used to study fluid–structure interactions and has not been applied to metal cutting yet. The CEL technique has, however, already been used and validated to model problems in solid mechanics. Skrzat (Skrzat, 2012) presents a benchmark of a 3-point bending flexural test of a beam of rectangular section. The comparison with a Lagrangian model gives similar results. Henke and Grabe (Henke and Grabe, 2011) show the results of a benchmark in geomechanics. The CEL model is opposed to analytical and Lagrangian results. Both models are similar to the analytical reference (the difference is of the order of 8%). Henke and Grabe (Henke and Grabe, 2011) note that the CEL method is well suited to solve problems involving large deformations for which difficulties arise when using the classical Lagrangian method. They also highlight the mesh sensitivity of the method. The CEL formulation is adopted by Smojver and Ivancevic (Smojver and Ivancevic, 2011) as well to solve successfully a bird strike damage analysis in an aircraft structure. Puls et al (Puls et al., 2014) use the CEL method to model a friction test and calibrate the friction model they introduce. In metal forming, Skrzat (Skrzat, 2012) develops CEL models to solve backward extrusion for symetric and non-symetric parts that could not be (or with many difficulties) with a Lagrangian approach.

In this paper, the CEL method is applied to the orthogonal cutting of the titanium alloy Ti6Al4V. The tool will described by a Lagrangian formulation and the workpiece by an Eulerian formulation. This will ensure that no mesh distortion issues occur and no chip separation criterion has to be introduced. The results of the CEL model will be compared to that of a classical ALE model and to experimental results obtained in strictly orthogonal cutting. The CEL model is well suited to solve transient problems and the ALE with pure Lagrangian boundaries flavor is selected for the ALE model (also suited to solve transient chip formation).

2. Experimental Ti6Al4V chip formation

A five-axis high speed milling machine Deckel-Maho DMU-80T was used, in dry cutting conditions, as a planning machine to remove a layer of material of variable, but larger than the tool edge radius, thickness. Thanks to this configuration (Fig. 1), introduced in (Ducobu et al., 2015a), the cutting is strictly orthogonal and the results can directly be compared to modeling.

The cutting speed, i.e. the feed rate of the machine, was set to the maximum achievable value, 30 m/min. This value is in the range recommended by the tool manufacturer SECO for the standard version of the tool and Ti6Al4V (27–39 m/min) (SECO TOOLS, 2011). The tool was placed on the machine table through an interface part fixed on the force sensor. This tool is custom made by SECO from standard element (LCGN160602-0600-GX-X, CP500) to machine radial grooves by turning (SECO TOOLS, 2011) in order to provide a rake angle of 15°, a clearance angle 2° and a cutting edge radius 20 μm, as in the experiments of Sun et al (Sun et al., 2009). and the numerical model used in (Ducobu et al., 2014). Three depths of cut, h, were considered: 100 μm, 60 μm and 40 μm. The cutting conditions of the experimental tests are summarized in Table 1. The cutting forces were measured in the three directions with a Kistler 9257B dynamometer at the sampling frequency of 70 kHz. The rest of the acquisition chain was composed of the multichannel charge amplifier Kistler 5070A, the data acquisition system (DAQ) Kistler 5697A2 and the DynoWare software.

The chips produced by the tests were collected and then observed with an optical microscope. They were embedded into epoxy resin to stand on their edge before being polished straight

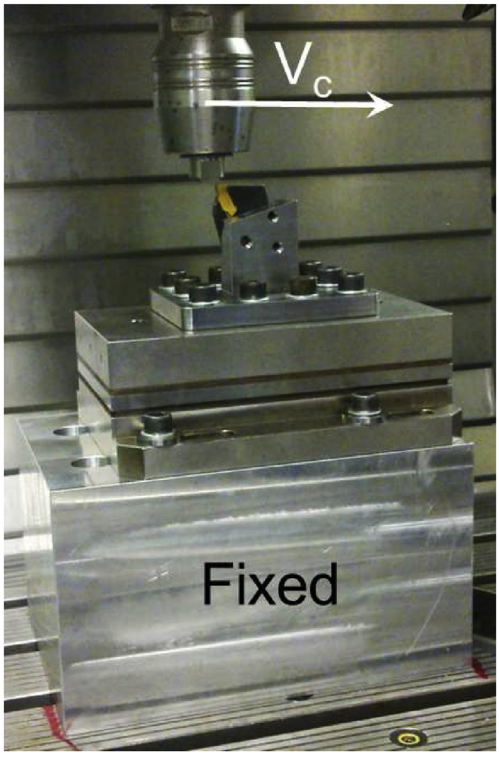

Fig. 1. Cutting configuration on the milling machine (Ducobu et al., 2015a).

Table 1
Cutting conditions of the experiments (Ducobu et al., 2015a).

Cutting speed (m/min)	30	
Depths of cut (μm)	100	6 repetitions
	60	6 repetitions
	40	3 repetitions
Width of cut (mm)	1	
Length of cut (mm)	10	
Rake angle (°)	15	
Clearance angle (°)	2	
Cutting edge radius (μm)	20	

across their length. They were then etched during about 45 s by Kroll's reagent to reveal the Ti6Al4V microstructure by coloring the β phase in dark brown (the darker color on the black and white microscope views).

The three chips are shown in Fig. 2 (a) to (c) at a magnification factor of 200. They are continuous chips and the one at 40 μm seems to have more very small and irregular teeth along its entire length than the two others (Fig. 2 (d)). The chips were not deformed during the unrolling preceding the embedding thanks to the small cutting length (10 mm), providing short and not rolled up chips. No error from that operation arises allowing to directly compare experimental and numerical geometrical values.

To characterize the chip morphologies, their thickness, h', was measured. The mean and standard deviation values are presented in Table 2 for 25 measurements on each chip. The chip compression ratio, λ_h, is given by (Toenshoff and Denkena, 2013)

$$\lambda_h = \frac{h'}{h} \tag{1}$$

The link between the chip compression ratio, λ_h, the rake angle, γ, and the shear angle, ϕ, is (Toenshoff and Denkena, 2013)

$$\lambda_h = \frac{\cos(\gamma - \phi)}{\sin\phi} \tag{2}$$

And the shear angle, ϕ, is directly given by

Table 2
Chip thickness at the three depths of cut for 25 measurements, h', chip compression ratio, λ_h, and shear angle, ϕ.

	100 μm	60 μm	40 μm
h' (μm)	135 ± 6	80 ± 4	59 ± 5
λ_h	1.35	1.34	1.48
ϕ (°)	63.5	63.2	66.7

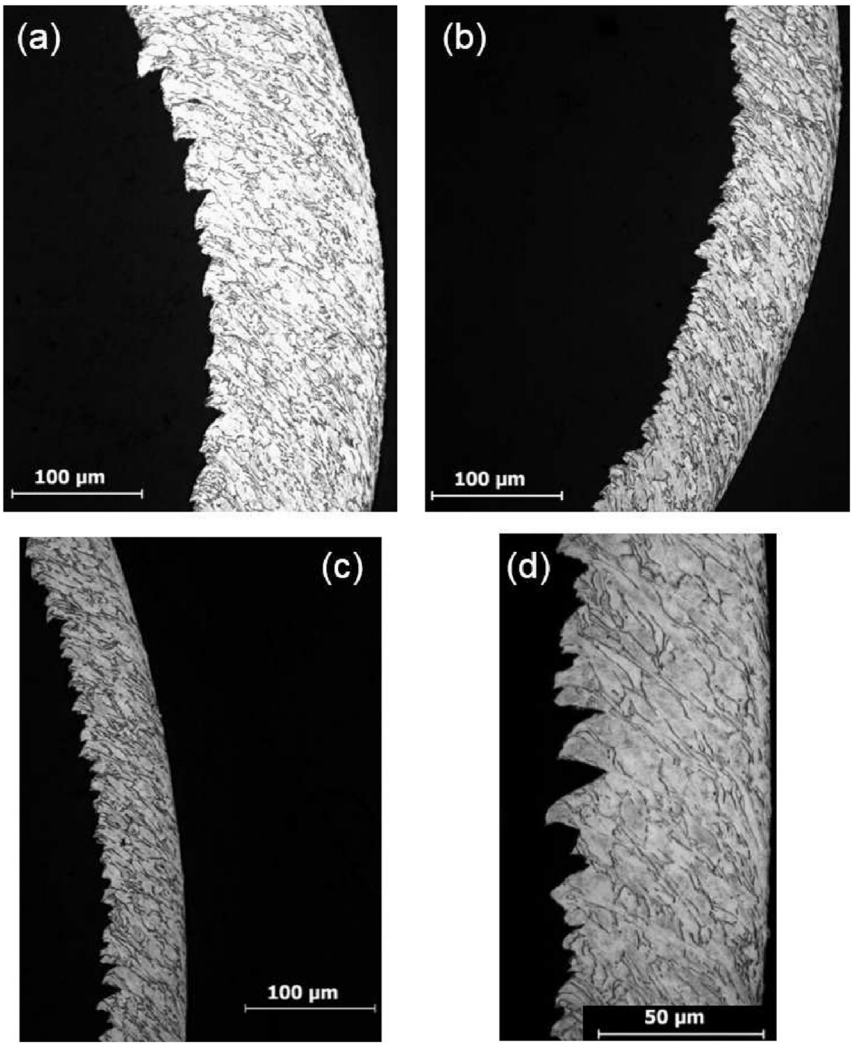

Fig. 2. Chips on optical microscope (a) 100 μm, (b) 60 μm, (c) 40 μm and (d) 40 μm at higher magnification factor (Ducobu et al., 2015a).

$$\tan\phi = \frac{\lambda_h \cos\gamma}{1 - \lambda_h \sin\gamma} \quad (3)$$

The values of the chip compression ratio and the shear angle are also given in Table 2. They are equal for the depths of cut of 100 μm and 60 μm, while their value is slightly higher at 40 μm. The standard deviation of the chip thickness is larger for that depth of cut by comparison to the two other ones (8.5% of the chip thickness versus around 5%); it is linked to the presence of the very small teeth on the 40 μm chip. The standard deviation of the chip thickness remains, however, small in the three cases.

The chip is continuous at the three depths of cut and therefore the cutting and feed forces are nearly constant and present smaller variations, as expected. The average value of the force in the direction perpendicular to the cutting plane is close to zero, confirming that the cut is orthogonal and not oblique. The cutting and feed forces are plotted for the depth of cut of 60 μm in Fig. 3. The measured signal has been filtered with a low-pass Butterworth filter with a cutoff frequency at 2 kHz (the first natural frequency of the Kistler dynamometer is of the order of 3.5 kHz). A higher level of the forces is observed at the beginning of the test. It is due to the entrance of the tool in the workpiece which is similar to an impact on the tool.

Table 3 summarizes the average root mean square (RMS) values of the forces for each cutting condition. The values presented are averaged on six measurements for the depths of cut of 100 μm and 60 μm and three measurements for 40 μm. As expected, the lower the depth of cut, the lower the level of the forces. It is interesting to note the increasingly influence of the tool edge radius on the cutting process: the ratio of the mean RMS values ($\frac{FF}{CF}$) increases, showing that the feed force decreases less quickly than the cutting force with the depth of cut.

3. Numerical models

3.1. CEL

The CEL method is only implemented in 3D in Abaqus/Explicit v6.11-3 (H.K.S., 2011). The CEL model developed will therefore be a tridimensional one. From a general point of view, that type of model is composed of an Eulerian mesh representing the volume in which the Eulerian material "flows" and interacts with Lagrangian part(s). Attention must be paid to the Eulerian mesh

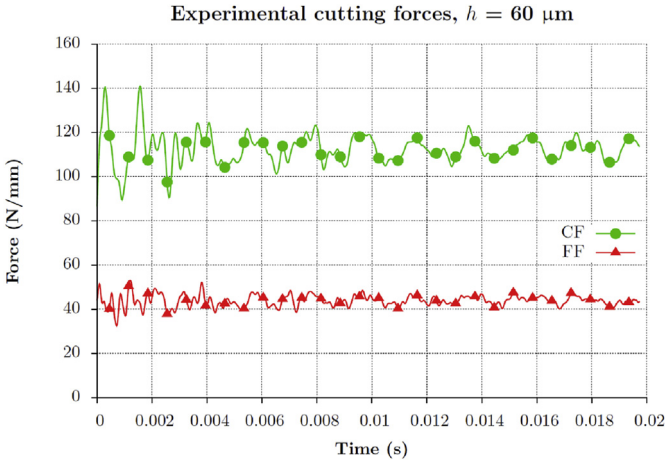

Fig. 3. Experimental cutting forces (cutting force, CF, and feed force, FF) at a cutting speed of 30 m/min and a depth of cut of 60 μm.

Table 3
Experimental cutting forces summary (6 repetitions at 100 μm and 60 μm, and 3 repetitions at 40 μm).

h (μm)	RMS CF (N/mm)	RMS FF (N/mm)	$\frac{FF}{CF}$
100	174 ± 2	50 ± 1	0.29
60	113 ± 2	44 ± 1	0.39
40	86 ± 2	40 ± 1	0.47

definition (Smojver and Ivancevic, 2011; H.K.S., 2011): the covered volume should be large enough to prevent the Eulerian material to flow out of it and be lost for the simulation. At the beginning of a CEL simulation, a fraction of the Eulerian mesh is usually filled with material, while the rest contains void. During the computation, the Eulerian Volume Fraction (EVF) is tracked for each element of the Eulerian mesh. It represents the ratio of material inside an element on the volume of that element (Smojver and Ivancevic, 2011; H.K.S., 2011). The EVF is a measure of how the element is "filled" of material: EVF = 1 means an element completely filled of material and EVF = 0 is an element empty of material ("full of void"). The penalty contact algorithm (Benson and Okazava, 2004) is used in Abaqus to handle contact in CEL analysis (Henke and Grabe, 2011; Smojver and Ivancevic, 2011; H.K.S., 2011).

In order to limit the number of degrees of freedom and thus the CPU computing time, as only 3D elements are available in Abaqus/Explicit v6.11-3, one element is used out of the cutting plane. The aim is to have a tridimensional model as close as possible to a bidimensional one to allow the comparison with a 2D plane strain model already validated (Ducobu et al., 2014). To avoid any displacement out of the plane, the normal displacements (to that plane) of the nodes of both lateral faces of the tool have been constrained. The workpiece is an Eulerian part and its displacement cannot be constrained. A zero-speed boundary condition has therefore been applied. The other boundary conditions are similar to these of a classical Lagrangian model (cf. 3.2): the workpiece is fixed in space while the tool moves towards the workpiece at the cutting speed; they are presented in Fig. 4.

The geometry of the Lagrangian tool is set to have the same angles (rake angle of 15° and clearance angle of 2°) and cutting edge radius (20 μm) than in the experiments. The Eulerian formulation of the workpiece leads to some specific features. The workpiece is defined as the volume in which Ti6Al4V can be found, whether it be the workpiece itself or the chip. It is therefore much higher than in a Lagrangian model. Moreover, Abaqus user's manual (H.K.S., 2011) recommends to place the Lagrangian part (the tool) that is supposed to contact the Eulerian one (the

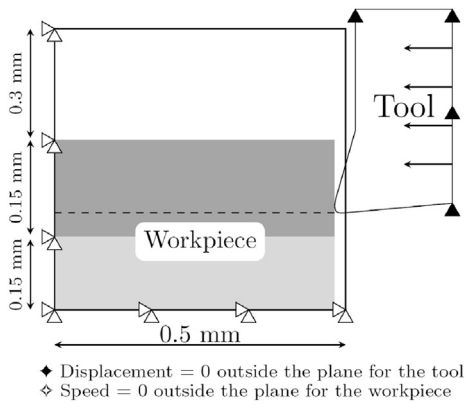

Fig. 4. Initial geometry and boundary conditions of the CEL model.

workpiece) inside the Eulerian mesh at the beginning of the simulation to help the calculation. A vertical narrow band (0.05 mm long) is therefore added at the right side of the workpiece, as shown in Fig. 4. The initial EVF are then defined to set where Ti6Al4V is inside the Eulerian mesh. The initial material distribution is illustrated in Fig. 4 where the gray areas show the presence of Ti6Al4V. That initial material distribution is the same for the three depths of cut considered, 100 μm, 60 μm and 40 μm, only the tool vertical position is modified. The length of the workpiece is set to 0.45 mm, which allows a cutting time of 550 μs while preventing the chip formation to be too close to the Eulerian mesh boundaries. Its total height is 0.6 mm, with 0.3 mm, three times the largest depth of cut, for the area initially filled with Ti6Al4V and 0.3 mm for the area initially filled with void.

The mesh is composed of 3D 8-node brick elements with a 5 μm × 5 μm square face in the cutting plane for the upper part of the workpiece filled with Ti6Al4V (Fig. 5, dark gray area in Fig. 4). This length is chosen to take into account the tool edge radius of 20 μm. The lower part and the area initially filled with void have coarser mesh, with the element size growing when getting closer to the mesh boundaries. The tool is composed of the same elements, but of variable length. The mesh is shown in Fig. 5, where the different densities can be seen. The model totals 5505 elements and 11,352 nodes (5428 elements and 11,160 nodes for the workpiece).

The behavior of Ti6Al4V is described by the Johnson–Cook (JC) constitutive model (Johnson and Cook, 1983). It is the most popular model used in cutting process simulation. Despite the appearance of several models taking the strain softening into account (Ducobu et al., 2015b), the JC model is still very used in the current literature (in (Miguèlez et al., 2013; Zhang et al., 2011b; Chen et al., 2011) for example). Taking the strain softening into account is needed to simulate a chip geometrically close to the experimental one when dynamic recrystallization, among others, occurs. This effect has a significant impact if a segmented (or sawtoothed) chip is formed, as it allows to produce a realistic chip and contributes to respect the physics of the formation of that kind of chips (Ducobu et al., 2014, 2015b). The experimental chips collected during the experimental tests are continuous. Describing the machined material by a constitutive model taking or not the strain softening into account will end in the same results. The JC model dissociates plastic, viscous and thermal aspects in three independent terms:

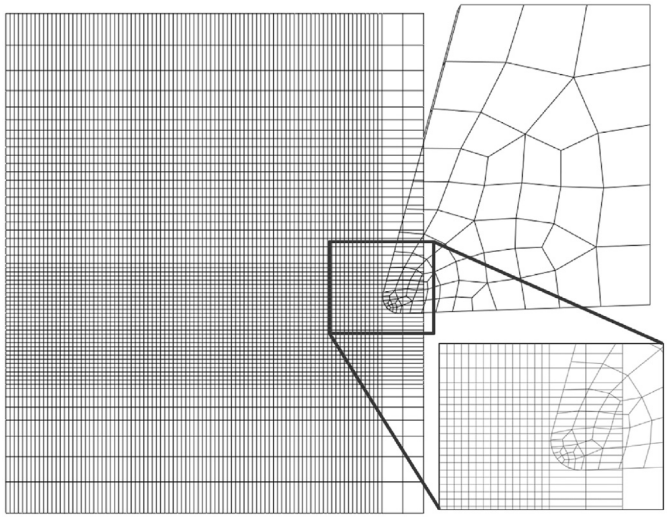

Fig. 5. Initial mesh of the CEL model.

$$\sigma = (A + B\varepsilon^n)\left(1 + C\ln\frac{\dot{\varepsilon}}{\dot{\varepsilon}_0}\right)\left(1 - \left[\frac{T - T_{room}}{T_{melt} - T_{room}}\right]^m\right) \quad (4)$$

where T_{melt} is the melting temperature, T_{room} is the room temperature and $\dot{\varepsilon}_0$ is the reference strain rate. A, B, C, m and n are material properties. Table 4 presents the set used for this study. According to Meyer and Kleponis (Meyer and Kleponis, 2001), the parameters where determined at strain rate levels of 0.0001 s^{-1}, 0.1 s^{-1} and 2150 s^{-1} and at a maximum plastic strain of 0.57. These Johnson–Cook parameters were selected for this study as the value of parameter A, 862 MPa, is equal to the yield stress of Ti6Al4V at room temperature (Meyer and Kleponis, 2001).

The tool material is tungsten carbide and its behavior is described by a linear elastic law. The materials properties of Ti6Al4V and tungsten carbide adopted in the numerical models are given in Table 4. Coulomb's friction is adopted to model friction at the tool–chip interface and all the friction energy is converted into heat. The coefficient value is extracted from (Calamaz et al., 2010) for the same tool – material couple. This simplified approach is still however widely adopted, particularly when the study is not focusing on wear and/or frictional aspect of the chip formation. It is classically assumed that the sharing of the heat generated by friction is carried out equally between the tool and the chip. This is confirmed experimentally by Rech et al (Rech et al., 2013). All the parts faces are adiabatic and the transformation of the deformation to heat is assumed to occur with an efficiency of 90% (Nasr et al., 2007).

3.2. ALE

The ALE model is intended to provide a numerical "conventional" reference. It consists of a 2D plane strain model derived from the one introduced in (Ducobu et al., 2014). The ALE method is chosen as it is quite close to the CEL method: the Eulerian formulation takes part in it and the chip separation criterion is not

Table 4
Material properties and cutting conditions of the numerical models (Özel and Zeren, 2007b; Meyer and Kleponis, 2001; Sun and Guo, 2009; Lampman, 1990; Calamaz et al., 2010).

JC constitutive model	A (MPa)	862
	B (MPa)	331
	C	0.012
	m	0.8
	n	0.34
	$\dot{\varepsilon}_0$	1
	T_{room} (K)	298
	T_{melt} (K)	1878
Inelastic heat fraction	Ti6Al4V	0.9
Density, ρ (kg/m^3)	Ti6Al4V	4430
	Carbide	15,000
Young's modulus, E (GPa)	Ti6Al4V	113.8
	Carbide	800
Expansion, α (K^{-1})	Ti6Al4V	8.6 e^{-6}
	Carbide	4.7 e^{-6}
Conductivity, k (W/mK)	Ti6Al4V	7.3
	Carbide	46
Specific heat, c_p (J/KgK)	Ti6Al4V	580
	Carbide	203
Friction coefficient		0.3
Friction energy to heat (%)		100
Heat partition to part (%)		50
Cutting speed (m/min)		30
Depths of cut (μm)	100, 60, 40	
Rake angle (°)		15
Clearance angle (°)		2
Cutting edge radius (μm)		20

necessary to form a chip. The cutting conditions, tool geometry and materials properties, given in Table 4, are the same as for the CEL model and the experiments. The heat transfer between the tool and the workpiece is, contrary to the CEL model, taken into account. The workpiece is modeled as rectangular block (Fig. 6) with a length and a height of 0.45 mm and 0.3 mm, respectively. These are the same values as that of the area filled with Ti6Al4V at the beginning of the simulation in the CEL model.

A uniform mesh of 5 μm square elements is used for the workpiece (Fig. 7), again to take the edge radius of the tool (20 μm) into account. The tool is composed of 4-node elements as well, but of variable length although identical to that of the CEL tool. The meshes of the tools and the upper part of the workpiece are therefore the same for both models. The ALE model is composed of 5473 elements and 5643 nodes (5400 elements and 5551 nodes for the workpiece). The total numbers of elements for both models are quite close and the difference in the numbers of nodes is due to the CEL model being tridimensional.

4. Results

For the results visualization with the CEL model, the user can choose to only show the elements filled with Ti6Al4V (see Fig. 8 (d) to (f)) and vice versa.

All the numerical chips are continuous, as shown in Fig. 8. The type of chips obtained with the models are therefore the same as that obtained experimentally (Fig. 2). Differences are however observed between the modeling and the experiments, but also between the models. In Fig. 8 (d), (e) and (f), the CEL chips seem longer, less rigid and their edges are more rounded (the more rounded geometry obtained with the CEL technique was already observed by (Skrzat, 2012)); these chips look more realistic and particularly those at 40 μm and 60 μm.

The chip thickness, chip compression ratio and shear angle for each depth of cut and model are given in Table 5. At 100 μm, both models overestimate the chip thickness. The difference is significant for ALE: 36% and smaller for CEL: 18%. At 60 μm, the chip thickness is still overestimated by the models. The CEL prediction is again better than the ALE one for this depth of cut: 16% versus 38% of difference with the experiments. At 40 μm, the experimental and CEL chip thicknesses are the same while the ALE one is overestimated by 22%. A potential source of error between the experiments and the modeling is that the lateral expansion of the chip (side flow) is neglected in both models as they are two dimensional ones. The experiments, while being in strictly orthogonal cutting conditions, are in a three dimensional configuration; allowing the chip to slightly expands laterally. This ends to a lower value of the chip thickness by comparison to a 2D model with a fixed chip width. This may explain, at least partially, why the numerical chip thicknesses are larger than the experimental values.

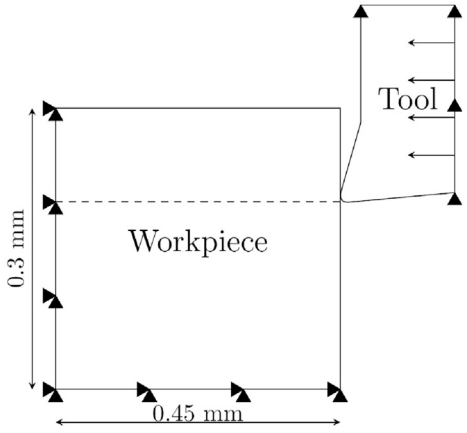

Fig. 6. Initial geometry and boundary conditions of the ALE model.

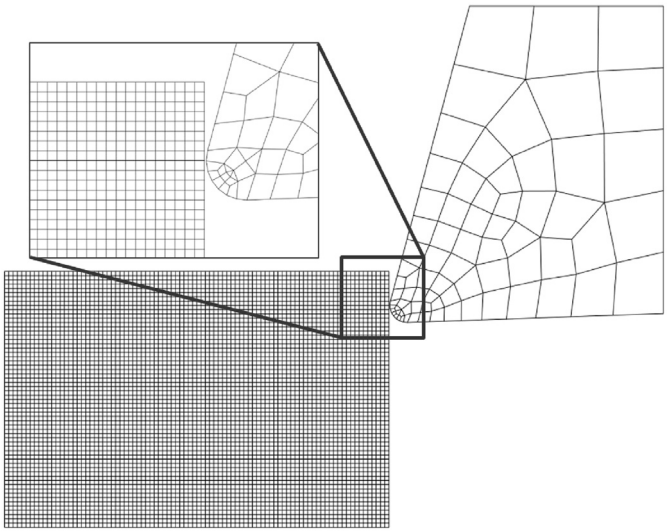

Fig. 7. Initial mesh of the ALE model.

The chip compression ratios and the shear angles follow the same trends concerning the values. About the evolutions of the chip compression ratio and the shear angle with the depth of cut, differences are noticed. The experimental values at 100 μm and 60 μm are very close and they increase at 40 μm. For the ALE model, the values are the same as well for the two larger depths of cut but they slightly decrease at 40 μm, contrary to the experiments. The CEL model leads to values decreasing with the depth of cut, which can be explained by the growing influence of the tool edge radius on the chip formation, similar to the decrease of the rake angle. This was, however, not observed experimentally. The CEL model seems therefore to be more sensitive to the depth of cut value on that point and to give better results when it is smaller. The results provided by the CEL model concerning the chip morphology are finally better than these of the ALE model.

The temperature contours are plotted in Fig. 8 and the maximal values after 550 μs of simulation are provided in Table 6. Temperatures given in Table 6 are rounded to the nearest ten. No experimental data is available and the objective is to compare the numerical values with the same hypothesis. The temperature is larger for the three models with the CEL formulation but the difference decreases with the depth of cut and the values are nearly equal at 40 μm. Except for that, contours near the tool rake face and under the machined surface are found very similar for the three depths of cut and the highest temperature is always situated in the secondary shear zone. It is noted that the temperatures are slightly higher in the tool for the ALE model.

Fig. 9 shows the cutting and the feed forces of both models at the depth of cut of 60 μm. As expected, due to the continuous chip produced, they are nearly constant. The forces evolutions are similar for the two other depths of cut. The forces obtained with the ALE model take more time than with the CEL model to reach their regime level.

The forces of the ALE model are slightly larger than that of the CEL model, which is partially due to the temperature difference between both models. Table 7 shows that it is the same for the two other depths of cut and that the forces measured experimentally are always larger than these of the modeling. The differences with

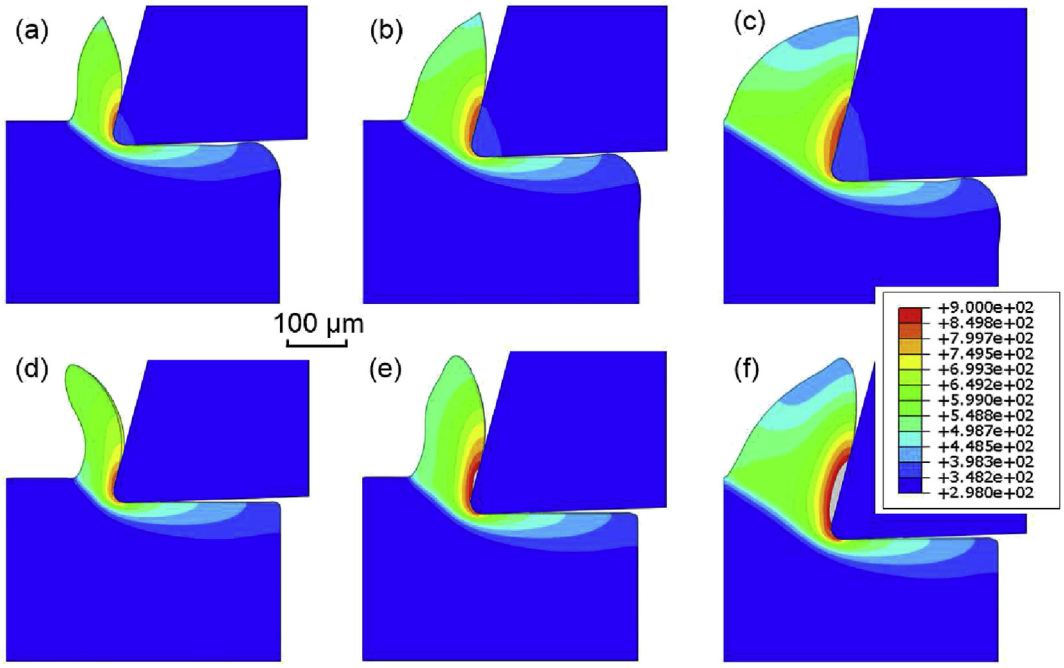

Fig. 8. Temperature contours (in K) of the numerical chips (a) ALE model at 40 µm, (b) ALE model at 60 µm, (c) ALE model at 100 µm, (d) CEL model at 40 µm, (e) CEL model at 60 µm and (f) CEL model at 100 µm.

Table 5
Chip thickness, h', chip compression ratio, λ_h, shear angle, ϕ, and difference with the experiments for the chip thickness, Δ (experiments: 25 values, modeling: 7 values).

h (µm)	Case	h' (µm)	Δ (%)	λ_h	ϕ (°)
100	Exp.	135 ± 6	–	1.35	63.5
	ALE	184 ± 2	−36	1.84	73.6
	CEL	160 ± 3	−18	1.60	69.2
60	Exp.	80 ± 4	–	1.34	63.2
	ALE	110 ± 1	−38	1.84	73.6
	CEL	93 ± 1	−16	1.55	68.2
40	Exp.	59 ± 5	–	1.48	66.7
	ALE	72 ± 1	−22	1.79	72.8
	CEL	59 ± 1	0	1.47	66.5

the experimental values range between 12% and 26% for the cutting force which is still acceptable. As usual in numerical modeling of metal cutting, the differences with the feed force are larger (difference with the experiments between 18% and 36%). The main reason for the difference in the cutting forces is the choice of the constitutive model of the material and the set of parameters adopted, as highlighted by Umbrello et al (Umbrello, 2008). and Ducobu et al (Ducobu et al., 2016). Feed forces closer to the experiments should be obtained for other friction conditions (coefficient as well as law) (Calamaz et al., 2008). The decrease of the cutting force with the depth of cut is observed in the experiments as well as in the modeling. The decrease of the feed force is experimentally lower and the numerical predictions give nearly

Table 6
Maximal temperature (°C) at 550 µs of simulation time.

Case	100 µm	60 µm	40 µm
ALE	≈600	≈590	≈560
CEL	≈730	≈660	≈570

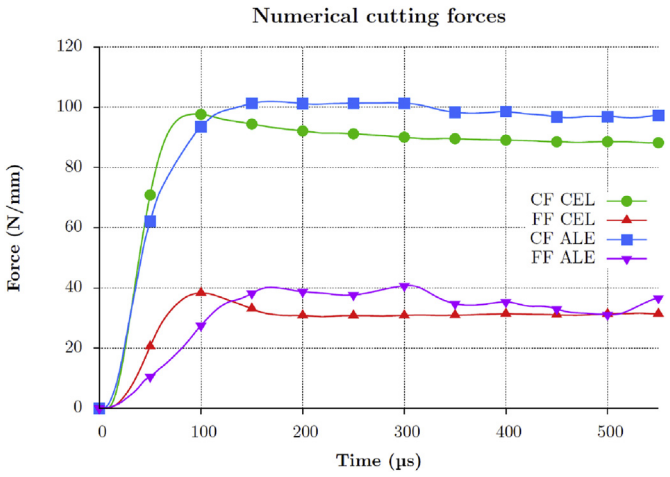

Fig. 9. Numerical cutting forces (cutting force, CF, and feed force, FF) at a cutting speed of 30 m/min and a depth of cut of 60 µm, low-pass filter cutoff frequency at 10 kHz.

Table 7
RMS cutting forces summary (experiments: 6 repetitions at 100 µm and 60 µm, and 3 repetitions at 40 µm), Δ_x: difference with the experimental values.

h (µm)	Case	CF (N/mm)	Δ_{CF} (%)	FF (N/mm)	Δ_{FF} (%)	$\frac{FF}{FF}$
100	Exp.	174 ± 2	–	50 ± 1	–	0.29
	ALE	150	14	36	28	0.24
	CEL	144	17	32	36	0.22
60	Exp.	113 ± 2	–	44 ± 1	–	0.39
	ALE	99	12	36	18	0.36
	CEL	90	20	31	30	0.34
40	Exp.	86 ± 2	–	40 ± 1	–	0.47
	ALE	72	16	33	18	0.46
	CEL	64	26	32	20	0.50

constant values versus the depth of cut. The increase of the cutting force on the feed force ratio when the depth of cut decreases observed experimentally, due to the growing influence of the tool edge radius on the chip formation, is reproduced by both models. That ratio value is larger for the CEL model at 40 μm, as expected when looking back at its higher sensitivity to the cutting edge radius of the tool. The CEL model gives therefore good results concerning the cutting forces.

The experimental machined length is 10 mm, while it is 0.275 mm in the models. The comparison between (close to steady-state) experimental and numerical results with a transient model is a classical issue for the validation of a finite element model. The representativeness of the experimental values has been checked, as well as the validity of the experimental – numerical comparison. The experimental chips have a similar geometry to what is presented in Fig. 2 on their whole length. The RMS values of the experimental and numerical forces do not take the entrance of the tool in the workpiece into account and after this entrance, all the forces are nearly constant (as it can be seen in Figs. 3 and 9). The temporal forces evolutions (Figs. 3 and 9) clearly show that they slightly oscillate around a mean value. It is therefore reasonable to consider that the steady-state has been reached for the chip morphology and the cutting forces. Concerning the temperatures, the values cannot be considered as steady-state values as the process has just started. It has more importance for the tool than for the workpiece as the temperature increase in the tool is mainly due to conduction inside of it. This aspect has no influence on the results presented in this paper. It would influence the results of a study focused on the tool wear for example.

The CPU computing time is also an important factor in metal cutting modeling, as it is still often very large (Davim, 2008, 2012). With the CEL model, 12 h 13 min were needed to compute 550 μs of simulation for the depth of cut of 60 μm on a single 2.5 GHz CPU and 8 GB of RAM. This time grows to 15 h 22 min for the ALE model. Such a result was not expected as the number of nodes is larger for the CEL model. However, as shown in Fig. 10, the stable time increment is larger in the CEL computation and it remains constant after a slight decrease at the beginning of the computing. For the ALE model, the computing starts with a lower stable time incrementation value but, thanks to the lower number of nodes, the CPU computing time is lower than for the CEL model (the CPU time to solve an increment is smaller, which balances the higher number of increments). Due to the elements deformation (although lower than in a Lagrangian model), the stable time increment decreases and after 450 μs of simulation, it takes more time to solve the ALE model than the CEL one. The evolution shapes of the CPU computing time versus the simulation time are different depending on the model (linear for CEL and looking exponential for ALE). The advantage of the absence of mesh deformation is clearly seen in this case and even allows to get results faster than with the ALE model. This should not be seen as a generality (CEL is faster than ALE) but more the advantage to keep the stable time increment constant. The use of mass scaling (Ducobu et al., 2015c; Cocchetti et al., 2012; Olovsson et al., 2005; Prior, 1994) could help to reduce the CPU computing time in both cases.

A lower number of increments is also an advantage for the precision of the solution given by the numerical model. The more increments are needed, the more the errors will increase. As an order of magnitude, of the order of 1,800,000 increments were needed to compute 550 μs of simulation with the CEL model, while nearly 3,900,000 increments were for the ALE one (Abaqus recommends, as far as possible, to stay below 2,000,000 increments to limit numerical errors due to the computing (H.K.S., 2011)). The CEL model is in the end more computing efficient than the ALE model.

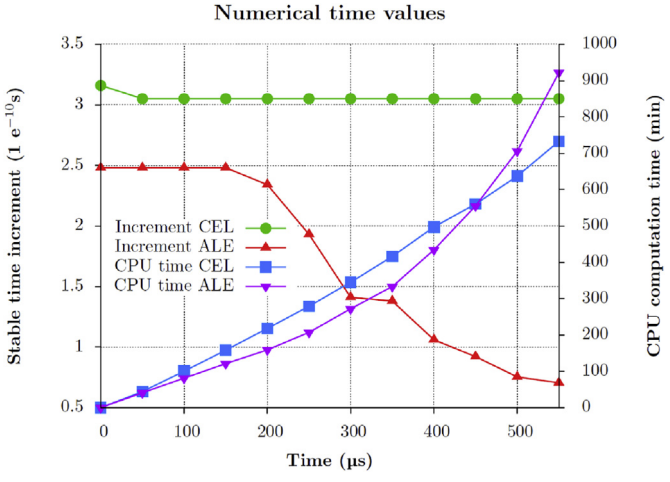

Fig. 10. Evolutions of the ALE and CEL stable time increments and CPU computing times versus simulation time, depth of cut of 60 μm.

5. Conclusions

The CEL formulation has been adopted to model the orthogonal cutting of Ti6Al4V at different depths of cut. The results were compared to that of an ALE model with Lagrangian boundaries and experimental results in strictly orthogonal cutting. They showed that the CEL model gives results close to both and that the tendencies when the depth of cut decreases are globally well captured. The chip morphology was similar to the experimental one and looked more "natural" than with the ALE formulation for small depths of cut. The forces were correctly estimated by the CEL model, although slightly lower than with the ALE method. The absence of element deformation in the workpiece, thanks to the Eulerian formulation is a significant advantage of the method. In the studied case, it can even lead to a CPU computing time smaller than with the ALE model because of the absence of stable time increment decrease due to the mesh deformation. These promising results obtained for the formation of a continuous chip should be expanded to other cutting conditions, "harder" to solve numerically, such as these leading to segmented (or saw-toothed) chips, but also other materials, materials constitutive models and friction modeling.

References

Arrazola, P., Özel, T., 2010. Investigations on the effects of friction modeling in finite element simulation of machining. Int. J. Mech. Sci. 52, 31–42.
Arrazola, P.J., Villar, A., Ugarte, D., Marya, S., 2007. Serrated chip prediction in finite element modeling of the chip formation process. Mach. Sci. Technol. 11, 1–24.
Arrazola, P.J., Ugarte, D., Dominguez, X., 2008. A new approach for the friction identification during machining through the use of finite element modeling. Int. J. Mach. Tools Manuf. 48, 173–183.
Arrazola, P., Özel, T., Umbrello, D., Davies, M., Jawahir, I., 2013. Recent advances in modelling of metal machining processes. CIRP Ann. Manuf. Technol. 62, 695–718.
Arrazola, P., Kortabarria, A., Madariaga, A., Esnaola, J., Fernandez, E., Cappellini, C., Ulutan, D., Özel, T., 2014. On the machining induced residual stresses in IN718 nickel-based alloy: experiments and predictions with finite element simulation. Simul. Model. Pract. Theory 41, 87–103.
Bäker, M., Rosler, J., Siemers, C., 2002. A finite element model of high speed metal cutting with adiabatic shearing. Comput. Struct. 80, 495–513.
Benson, D., Okazava, S., 2004. Contact in a multi-material eulerian finite element formulation. Comput. Methods Appl. Mech. Eng. 193, 4277–4298.
Calamaz, M., Coupard, D., Girot, F., 2008. A new material model for 2D numerical simulation of serrated chip formation when machining titanium alloy Ti-6Al-4V. Int. J. Mach. Tools Manuf. 48, 275–288.
Calamaz, M., Coupard, D., Girot, F., 2010. Numerical simulation of titanium dry machining with a strain softening constitutive law. Mach. Sci. Technol. 14,

244–257.
Chen, G., Ren, C., Yang, X., Jin, X., Guo, T., 2011. Finite element simulation of high-speed machining of titanium alloy (ti-6al-4v) based on ductile failure model. Int. J. Adv. Manuf. Technol. 56, 1027–1038.
Cocchetti, G., Pagani, M., Perego, U., 2012. Selective mass scaling and critical time-step estimate for explicit dynamics analyses with solid-shell elements. Comput. Struct 127, 39–52. http://dx.doi.org/10.1016/j.compstruc.2012.10.021.
Courbon, C., Mabrouki, T., Rech, J., Mazuyer, D., D'Eramod, E., 2013. On the existence of a thermal contact resistance at the tool-chip interface in dry cutting of AISI 1045: formation mechanisms and influence on the cutting process. Appl. Therm. Eng. 50, 1311–1325.
Davim, J. (Ed.), 2008. Machining: Fundamentals and Recent Advances. Springer.
Davim, J.P. (Ed.), 2012. Statistical and Computational Techniques in Manufacturing. Springer.
Davim, J.P., Maranhão, C., 2009. A study of plastic strain and plastic strain rate in machining of steel AISI 1045 using FEM analysis. Mat. Des. 30, 160–165.
Ducobu, F., Rivière-Lorphèvre, E., Filippi, E., 2014. Numerical contribution to the comprehension of saw-toothed Ti6Al4V chip formation in orthogonal cutting. Int. J. Mech. Sci. 81, 77–87.
Ducobu, F., Rivière-Lorphèvre, E., Filippi, E., 2015. Experimental contribution to the study of the Ti6Al4V chip formation in orthogonal cutting on a milling machine. Int. J. Mater. Form. 8, 455–468.
Ducobu, F., Arrazola, P.-J., Rivière-Lorphèvre, E., Filippi, E., 2015. Comparison of several behaviour laws intended to produce a realistic Ti6Al4V chip by finite elements modelling. Key Eng. Mater. 651–653, 1197–1203.
Ducobu, F., Rivière-Lorphèvre, E., Filippi, E., 2015. On the introduction of adaptive mass scaling in a finite element model of Ti6Al4V orthogonal cutting. Simul. Model. Pract. Theory 53, 1–14.
Ducobu, F., Rivière-Lorphèvre, E., Filippi, E., 2016. Material constitutive model and chip separation criterion influence on the modeling of Ti6Al4V machining with experimental validation in strictly orthogonal cutting condition. Int. J. Mech. Sci. 107, 136–149.
Ghadbeigi, H., Bradbury, S., Pinna, C., Yates, J., 2009. On the modelling of chip formation in orthogonal cutting: damage mechanics approach. In: Proceedings of the 12th CIRP Conference on Modeling of Machining Operations, pp. 77–82.
Heinstein, M., Segalman, D., 1997. Simulation of Orthogonal Cutting with Smooth Particle Hydrodynamics. Technical Report. Sandia National laboratories.
Henke, G.Q.S., Grabe, J., 2011. Application of a coupled eulerian-lagrangian approach on geomechanical problems involving large deformations. Comput. Geotech. 38, 30–39.
H.K.S., 2011. Abaqus Analysis User's Manual, Version 6.11. Dassault Systèmes.
Jackson, M., Whitfield, M., Morrell, J., Davim, J.P., 2010. Computational analysis of the intimate contact between an inclined wedge and low carbon steel during metal cutting. Int. J. Mater. Prod. Technol. 37, 2–29.
Johnson, G., Cook, W., 1983. A constitutive model and data for metals subjected to large strains, high strain rates and high temperatures. In: Proceedings of the Seventh International Symposium on Ballistics, the Hague, The Netherlands, pp. 541–547.
Lampman, S., 1990. Wrought titanium and titanium alloys, properties and selection: nonferrous alloys and special-purpose materials, ASM Handbook. ASM Int. 2, 592–633.
Li, K., Gao, X.-L., Sutherland, J., 2002. Finite element simulation of the orthogonal metal cutting process for qualitative understanding of the effects of crater wear on the chip formation process. J. Mater. Process. Technol. 127, 309–324.
Mabrouki, T., Rigal, J.-F., 2006. A contribution to a qualitative understanding of thermo-mechanical effects during chip formation in hard turning. J. Mater. Process. Technol. 176, 214–221.
Maranhão, C., Davim, J.P., 2010. Finite element modelling of machining of AISI 316 steel: numerical simulation and experimental validation. Simul. Model. Pract. Theory 18, 139–156.
Meyer, H., Kleponis, D., 2001. Modeling the high strain rate behavior of titanium undergoing ballistic impact and penetration. Int. J. Impact Eng. 26, 509–521.
Miguèlez, M., Soldani, X., Molinari, A., 2013. Analysis of adiabatic shear banding in orthogonal cutting of Ti alloy. Int. J. Mech. Sci. 75, 212–222.
Nasr, M., Ng, E.-G., Elbestawi, M., 2007. Effects of workpiece thermal properties on machining-induced residual stresses – thermal softening and conductivity. Proc. Inst. Mech. Eng. Part B J. Eng. Manuf. 221, 1387–1400.
Obikawa, T., Sasahara, H., Shirakashi, T., Usui, E., 1997. Application of computational machining method to discontinuous chip formation. J. Manuf. Sci. Eng. 119, 667–674.
Ohbuchi, Y., Obikawa, T., 2003. Finite element modeling of chip formation in the domain of negative rake angle cutting. ASME 125, 324–332.
Olovsson, L., Simonsson, K., Unosson, M., 2005. Selective mass scaling for explicit finite element analyses. Int. J. Numer. Meth. Eng. 63, 1436–1445.
Owen, D.R.J., Vaz Jr, M., 1999. Computational techniques applied to high-speed machining under adiabatic strain localization conditions. Comput. Methods Appl. Mech. Eng. 171, 445–461.
Özel, T., Zeren, E., 2005. Finite element method simulation of machining of AISI 1045 steel with a round edge cutting tool. In: Proceedings of 8th CIRP International Workshop on Modeling of Machining Operations, pp. 533–542.
Özel, T., Zeren, E., 2007a. Finite element modeling the influence of edge roundness on the stress and temperature fields induced by high-speed machining. Int. J. Adv. Manuf. Technol. 35, 255–267.
Özel, T., Zeren, E., 2007b. Numerical modelling of meso-scale finish machining with finite edge radius tools. Int. J. Mach. Mach. Mater. 2, 451–768.
Pantalé, O., 2005. Plateforme de prototypage virtuel pour la simulation numrique en Grandes Transformations Thermomcaniques Rapides. Technical Report. Institut National Polytechnique de Toulouse.
Pantalé, O., Bacaria, J.-L., Dalverny, O., Rakotomalala, R., Caperaa, S., 2004. 2D and 3D numerical models of metal cutting with damage effects. Comput. Methods Appl. Mech. Eng. 193, 4383–4399.
Prior, A.M., 1994. Application of implicit and explicit finite element techniques to metal forming. J. Mater. Process. Technol. 45, 649–656.
Puls, H., Klocke, F., Lung, D., 2014. Experimental investigation on friction under metal cutting conditions. Wear 310, 63–71.
Rech, J., Arrazola, P., Claudin, C., Courbon, C., Pusavec, F., Kopac, J., 2013. Characterisation of friction and heat partition coefficients at the tool-work material interface in cutting. CIRP Ann. Manuf. Technol. 62, 79–82.
Schulze, V., Zanger, F., 2011. Development of a simulation model to investigate tool wear in Ti-6-Al-4V alloy machining. Adv. Mater. Res. 223, 535–544.
SECO TOOLS, 2011. Turning Catalog and Technical Guide 2012. SECO TOOLS AB.
Simoneau, A., Ng, E., Elbestawi, M., 2006. Chip formation during microscale cutting of medium carbon steel. Int. J. Mach. Tools Manuf. 46, 467–481.
Simoneau, A., Ng, E., Elbestawi, M., 2007. Grain size and orientation effects when microcutting AISI 1045 steel. Ann. CIRP 56, 57–60.
Skrzat, A., 2012. Application of coupled eulerian-lagrangian approach in metal forming simulations. Mechanika 294, 25–35.
Smojver, I., Ivancevic, D., 2011. Bird strike damage analysis in aircraft structures using abaqus/explicit and coupled eulerian lagrangian approach. Compos. Sci. Technol. 71, 489–498.
Subbiah, S., Melkote, S., 2008. Effect of finite edge radius on ductile fracture ahead of the cutting tool edge in micro-cutting of Al2024-T3. Mater. Sci. Eng. A 474, 283–300.
Sun, J., Guo, Y.B., 2009. Material flow stress and failure in multiscale machining titanium alloy Ti-6Al-4V. Int. J. Adv. Manuf. Technol. 41, 651–659.
Sun, S., Brandt, M., Dargusch, M., 2009. Characteristics of cutting forces and chip formation in machining of titanium alloys. Int. J. Mach. Tools Manuf. 49, 561–568.
Toenshoff, H., Denkena, B., 2013. Basics of Cutting and Abrasive Processes. Springer Verlag.
Umbrello, D., 2008. Finite element simulation of conventional and high speed machining of Ti6Al4V alloy. J. Mater. Process. Technol. 196, 79–87.
Woon, K., Rahman, M., Fang, F., Neo, K., Liu, K., 2007. Investigations of tool edge radius effect in micromachining: a FEM simulation approach. J. Mater. Process. Technol. 167, 316–337.
Yvonnet, J., 2004. Nouvelles approches sans maillage bases sur le mthode des lments naturels pour la simulation numrique des procds de mise en forme. Ph.D. thesis. cole Nationale Suprieure d'Arts et Mtiers, Centre de Paris.
Zhang, Y., Mabrouki, T., Nelias, D., Gong, Y., 2011. FE-model for titanium alloy (Ti-6Al-4V) cutting based on the identification of limiting shear stress at tool-chip interface. Int. J. Mater. Form. 4, 11–23.
Zhang, Y., Mabrouki, T., Nelias, D., Gong, Y.D., 2011. Chip formation in orthogonal cutting considering interface limiting shear stress and damage evolution based on fracture energy approach. Finite Elem. Anal. Des. 47, 850–863.